



<http://www.diva-portal.org>

## Postprint

This is the accepted version of a paper published in *International Journal of Quantum Chemistry*. This paper has been peer-reviewed but does not include the final publisher proof-corrections or journal pagination.

Citation for the original published paper (version of record):

Zheng, G., Lundberg, M., Jakowski, J., Vreven, T., Frisch, M J. et al. (2009)  
Implementation and Benchmark Tests of the DFTB Method and Its Application in the ONIOM Method.  
*International Journal of Quantum Chemistry*, 109(9): 1841-1854  
<http://dx.doi.org/10.1002/qua.22002>

Access to the published version may require subscription.

N.B. When citing this work, cite the original published paper.

Permanent link to this version:

<http://urn.kb.se/resolve?urn=urn:nbn:se:uu:diva-145476>

## Implementation and benchmark tests of the DFTB method and its application in the ONIOM method

Guishan Zheng,<sup>1a</sup> Marcus Lundberg,<sup>2</sup> Jacek Jakowski,<sup>1</sup> Thom Vreven,<sup>3</sup> Michael J. Frisch,<sup>3</sup> Keiji Morokuma<sup>1,2\*</sup>

<sup>1</sup>Cherry Emerson Center for Scientific Computation and Department of Chemistry, Emory University, Atlanta, GA 30322

<sup>2</sup>Fukui Institute for Fundamental Chemistry, Kyoto University, Kyoto 606-8103, Japan

<sup>3</sup>Gaussian, Inc., 340 Quinpiac Street, Building 40, Wallingford, CT 06492

**Abstract:** We present the theoretical and implementation details of the DFTB method with analytical gradients into the Gaussian package. SCF optimization performance with DIIS method is compared with modified Broyden method and Anderson methods, from which DIIS method is to be preferred. The number of geometry optimization steps can be significantly decreased with the Broyden algorithm compared to the conjugated gradient method. From the comparison of geometry parameters as well as trends in the change of HOMO and LUMO energies, the results show clearly that DFTB can reproduce values obtained at the B3LYP/6-31G(d) level well. We also investigated the DFTB method as the low level quantum mechanical (QM) method in an ONIOM(QM:QM') description for an amino acid model system and found DFTB promising as a method to describe polarization and charge-transfer effects in large systems.

---

\*Corresponding Author: [morokuma@fukui.kyoto-u.ac.jp](mailto:morokuma@fukui.kyoto-u.ac.jp)

<sup>a</sup> Present address: Department of Chemistry and Chemical Biology, Harvard University, Cambridge, MA 02138

## 1. Introduction

Despite the rapid development of *ab initio* methods and density functional theory (DFT) and their widespread applications,<sup>1</sup> semiempirical methods are still used very frequently as they are usually 2-3 orders of magnitude faster than DFT or Hartree-Fock methods. Especially for quantum mechanical (QM) studies of very large systems, such as carbon nanotube molecules or biomolecular systems, containing hundreds to thousands of atoms, a semiempirical method is often the only affordable choice. With a careful parameterization, errors in semiempirical calculations are often within a qualitatively acceptable range. Consequently, efforts in the development and applications of semiempirical methods still continue more than three decades after their inception.<sup>2-29</sup> Semiempirical methods are also considered to be the low-level QM method in hybrid ONIOM(QM:QM') or ONIOM(QM:QM':MM) methods.<sup>30-34</sup> Furthermore, semiempirical methods can be used in QM dynamics calculations for medium sized systems<sup>35-41</sup> or in QM/MM dynamics for large systems.<sup>33,34,42</sup>

In conventional semiempirical methods, i.e. those derived from the Hartree-Fock theory, the neglect of diatomic differential overlap (NDDO) approximation is adopted in many semiempirical methods, including MNDO,<sup>3</sup> AM1,<sup>5</sup> PM3.<sup>13</sup> With the recent reparameterization or explicit inclusion of the overlap matrix, newly developed methods like OM<sub>x</sub>,<sup>9,29</sup> PDDG/PM3,<sup>10</sup> and RM1<sup>14</sup> have significantly improved accuracy according to benchmark results of several groups.

Inspired by the success of the density functional theory in last two decades, a semiempirical method called *density functional based tight binding* (DFTB) was introduced a decade ago.<sup>26,27</sup> DFTB is a second order approximation of density functional theory that neglects multicenter integrals and uses a valence minimal basis set,<sup>43,44</sup> in the same spirit as many other semiempirical methods derived from the Hartree-Fock theory. However, all parameters in the DFTB method, e.g. the atomic Hubbard values, the core Hamiltonian matrix and the overlap matrix, are calculated with the PBE functional. In addition, the diatomic repulsion potential is determined from model calculations using B3LYP with a double zeta basis set.<sup>25</sup> The introduction of explicit

charge interaction, self-consistent charge DFTB (SCC-DFTB), has improved the reliability with respect to the version without charge interaction (NCC-DFTB), particularly for polar systems. Hereafter, DFTB is referred to as SCC-DFTB including spin polarization effects for nonzero spin states. The method has accuracy comparable with AM1 or PM3, which has been extensively tested and used for many years.<sup>8,11,24</sup> The success of the DFTB method in the prediction of geometries and energetics of organic molecules inspired us to extend the parameterization to the first row transition metal elements.<sup>25</sup>

In order to fully take advantage of the efficiency and accuracy of the DFTB method in a standard quantum chemistry code and to allow easier internal ONIOM adoption, we have implemented the DFTB method in the Gaussian package.<sup>45</sup> Due to its practical importance, we assessed the SCF convergence and geometry optimization performance of the DFTB method and compared several different algorithms. In addition, two-layer and three-layer ONIOM approaches have been tested for an amino acid model system, where the polarization and charge-transfer effects described by the DFTB method are emphasized. Theoretical background and implementation details will be introduced in section 2, followed by computational details in section 3. Results of test calculations and discussions will be presented in section 4, and the conclusion will be made in section 5.

## **2. Theoretical background and implementation details**

### **A. DFTB method**

There are several excellent review articles available with detailed descriptions of the theoretical aspects of the DFTB method as well as the most recent advances in theoretical development and application.<sup>43,44</sup> In this section, we present a (self-contained) summary with an emphasis on the aspects that are particularly relevant to our implementation.

**Total energy.** With the explicit consideration of charge and spin interaction on top of the two-center tight-binding approximation, the total DFTB energy of a molecule in the spin polarized (unrestricted) representation is given by<sup>28</sup>

$$E = \sum_{\sigma=\alpha,\beta} \sum_i^{occ} \langle \psi_i^\sigma | H^0 | \psi_i^\sigma \rangle + \frac{1}{2} \sum_{A,B}^{Atom} \gamma^{AB} \Delta q^A \Delta q^B + \frac{1}{2} \sum_A^{Atom} \sum_{l,l'} Q_l^A W_{ll'}^A Q_{l'}^A + \sum_{A>B}^{Atom} V^{AB}, \quad (1)$$

where  $\psi_i^\sigma$  is the  $i$ -th occupied orbital for spin  $\sigma$ ,  $H^0$  is the core Hamiltonian,  $\gamma^{AB}$  is a distance-dependent interaction parameter between the Mulliken charges  $\Delta q^A$  and  $\Delta q^B$  on atom A and B, respectively, and  $W_{ll'}^A$  is the one-center spin density interaction parameter on atom A between the Mulliken spin populations  $Q_l^A$  and  $Q_{l'}^A$  on orbitals with angular momentum  $l$  and  $l'$ , respectively.  $V^{AB}$  is the parameterized pair-wise interatomic repulsive potential. The molecular orbital  $\psi_i^\sigma$  for spin  $\sigma$  is given as a linear combination of localized pseudoatomic valence Slater orbitals

$$\psi_i^\sigma = \sum_{\mu}^{AO} c_{\mu i}^\sigma \chi_{\mu} \quad (2)$$

The density matrix element  $P_{\mu\nu}^\sigma$  for  $\sigma$  spin, the Mulliken population  $q^A$  and charge  $\Delta q^A$  on atom A, and the Mulliken spin population  $Q_l^A$  on orbitals with angular momentum  $l$  on atom A are defined by

$$\begin{aligned} P_{\mu\nu}^\sigma &= \sum_i^{occ} c_{\mu i}^\sigma c_{\nu i}^\sigma, \quad \sigma = \alpha, \beta \\ q^A &= \sum_{\mu \in A}^{AO} \sum_{\nu}^{AO} (P_{\mu\nu}^\alpha + P_{\mu\nu}^\beta) S_{\mu\nu}, \\ \Delta q^A &= q^A - Z^A \\ Q_l^A &= \sum_{\mu \in A}^{AO \text{ with } l} \sum_{\nu}^{AO} (P_{\mu\nu}^\alpha - P_{\mu\nu}^\beta) S_{\mu\nu} \end{aligned}, \quad (3)$$

where  $Z^A$  is the core charge of atom A, and  $S_{\mu\nu}$  is the overlap matrix element  $S_{\mu\nu} = \langle \chi_{\mu} | \chi_{\nu} \rangle$ .

Alternatively, for simplicity and efficiency in practical implementation, the DFTB total energy can be written as

$$E = \langle P^\alpha (h + F^\alpha) \rangle + \langle P^\beta (h + F^\beta) \rangle + E_{rep}, \quad (4)$$

where the bracket represents the matrix trace,  $E_{rep}$  is a sum of pairwise interatomic potentials

$$E_{rep} = \sum_{A>B}^{Atom} (V^{AB} + Z^A \gamma^{AB} Z^B), \quad (5)$$

$h$ ,  $P^\sigma$  and  $F^\sigma$  are the one-electron Hamiltonian matrix, density matrix for  $\sigma$  spin, and Fock matrix for  $\sigma$  spin, respectively. The Fock matrix is the sum of the one-electron Hamiltonian matrix  $h$  and the two-electron matrix  $G^\sigma$ :

$$F^\sigma = h + G^\sigma, \quad \sigma = \alpha, \beta. \quad (6)$$

The one-electron and two-electron matrix elements,  $h_{\mu\nu}$  and  $G_{\mu\nu}$ , for AO  $\mu$  on atom  $A$  with angular momentum  $l$  and AO  $\nu$  on atom  $B$  with angular momentum  $l'$  are given by:

$$h_{\mu\nu} = h_{\mu\nu}^0 - \frac{1}{2} S_{\mu\nu} \sum_C^{Atom} (\gamma^{AC} + \gamma^{BC}) Z^C, \quad (7)$$

$$G_{\mu\nu}^\sigma = \frac{1}{2} S_{\mu\nu} \left[ \sum_C^{Atom} (\gamma^{AC} + \gamma^{BC}) q^C + \delta_\sigma \left( \sum_{l''} W_{ll''}^A Q_{l''}^A + \sum_{l''} W_{l'l''}^B Q_{l''}^B \right) \right] \quad (8)$$

where  $h_{\mu\nu}^0$  is the core Hamiltonian matrix element, and

$$\delta_\sigma = \begin{cases} 1, & \text{for } \sigma=\alpha \\ -1, & \text{for } \sigma=\beta \end{cases}. \quad (9)$$

The initial guess density matrix can be generated from a variety of different approaches, e.g. Hückel method, core Hamiltonian and Harris functional.<sup>46</sup> The density matrix is then iteratively updated until all density matrix elements and the total electronic energy are converged within predetermined threshold values. The DFTB code described here has been implemented in such a way that many algorithms available in the Gaussian package can be utilized naturally. We note that the density matrix update in Gaussian is different from the SCF algorithm in the Paderborn DFTB code where the atomic Mulliken charges are updated via the Broyden method until the electronic energy is self-consistent between two consecutive iterations.

**Geometry optimization.** Geometry optimization is accomplished by the use of analytical

derivatives of the energy (gradients) with respect to the nuclear coordinates. From the energy formalism in the above section, the analytical energy gradient  $E^x$  with respect to the general Cartesian coordinate  $x$  is given by

$$E^x = \left\langle (P^\alpha + P^\beta) h^x \right\rangle + \frac{1}{2} \left\langle (P^\alpha G^{\alpha,x} + P^\beta G^{\beta,x}) \right\rangle - \left\langle Y S^x \right\rangle + E_{rep}^x \quad (10)$$

where  $h^x$  and  $G^x$  are the one-electron and two-electron matrix derivatives, respectively,  $S^x$  is the overlap matrix derivative and  $E_{rep}^x$  is the derivative of the sum of the pair wise repulsive potential energy terms, all with respect to  $x$ .  $Y$  is the energy weighted density matrix

$$Y = P^\alpha F^\alpha P^\alpha + P^\beta F^\beta P^\beta. \quad (11)$$

The one- and two-electron matrix derivative element is given by

$$h_{\mu\nu}^x = h_{\mu\nu}^{0,x} - \frac{1}{2} S_{\mu\nu}^x \left[ \sum (\gamma^{AC} + \gamma^{BC}) Z^C \right] - \frac{1}{2} S_{\mu\nu} \left[ \sum (\gamma^{AC,x} + \gamma^{BC,x}) Z^C \right]. \quad (12)$$

$$G_{\mu\nu}^{\sigma,x} = S_{\mu\nu}^x \left[ \sum_C^{Atom} (\gamma^{AC} + \gamma^{BC}) q^C + \delta_\sigma \left( \sum_{l''}^A W_{ll''}^A Q_{l''}^A + \sum_{l''}^B W_{l'l''}^B Q_{l''}^B \right) \right] + \frac{1}{2} S_{\mu\nu} \left[ \sum_C^{Atom} (\gamma^{AC,x} + \gamma^{BC,x}) q^C \right] \quad (13)$$

With the equations (11), (12), and (13), the computation of the energy gradient (10) can be assembled into the following compact form:

$$E^x = \sum_{A>B}^{Atom} (V^{AB,x} + \Delta q^A \gamma^{AB,x} \Delta q^B) + \sum_{\mu,\nu}^{AO} (P_{\mu\nu}^\alpha + P_{\mu\nu}^\beta) h_{\mu\nu}^{0,x} + \sum_{\mu,\nu}^{AO} S_{\mu\nu}^x \left[ Y_{\mu\nu} + \frac{1}{2} (P_{\mu\nu}^\alpha + P_{\mu\nu}^\beta) \sum_C^{Atom} (\gamma^{AC} + \gamma^{BC}) \Delta q^C + \frac{1}{2} (P_{\mu\nu}^\alpha - P_{\mu\nu}^\beta) \left( \sum_{l''}^A W_{ll''}^A Q_{l''}^A + \sum_{l''}^B W_{l'l''}^B Q_{l''}^B \right) \right] \quad (14)$$

where, in the second line,  $A$  and  $B$  in the square bracket refer to atoms to which AO  $\mu$  and  $\nu$  belong, respectively. The core Hamiltonian matrix derivative elements  $h_{\mu\nu}^{0,x}$  and  $S_{\mu\nu}^x$  are computed numerically with a central finite difference approximation. In geometry optimization, the structural symmetry can be fully accounted for.

Based on equation (1), the present implementation is general, and is applicable to the non-charge version (NCC-DFTB, neglecting contributions of charges and spin-densities) as well

as to the self-consistent charge version (SCC-DFTB) version, with spin-polarization (spin-unrestricted, including spin- $W_{ii}^A$  interaction) or without it (spin-restricted, neglecting spin- $W_{ii}^A$  interaction). The implementation was made and the test calculations below were performed using the Gaussian development version GDV F.02 package.<sup>45</sup>

## B. SCF and geometry optimization

**SCF.** For SCF optimization, there are various algorithms that have been widely applied in the quantum chemistry community, including level-shifting,<sup>47-51</sup> damping,<sup>52</sup> DIIS,<sup>53,54</sup> QC<sup>55</sup> and others. In DIIS, only a limited number of previous DIIS error vectors, which scales linearly with the number of basis function, need to be saved. This is of great practical importance for calculations on large systems because every SCF iteration requires  $O(N^3)$  effort ( $N$  is the number of basis function) for updating the Fock matrix elements and solving the SCF equations. More importantly, DIIS is quite robust due to its intrinsic numerical properties.<sup>56,57</sup> Especially, when energies of the initial few iterations are interpolated,<sup>54</sup> which is often called EDIIS, the convergence performance of DIIS is significantly improved. Consequently, the DIIS algorithm has been implemented in many quantum chemistry packages and is often the default choice. With the above consideration, Gaussian employs a combination of EDIIS at early iterations and then transits to conventional DIIS algorithm (CDIIS), which leads to an extremely efficient method in most practical calculations. In contrast, in the solid state physics community, the modified Broyden method and the Anderson method are employed by many groups.<sup>58</sup> In fact, DIIS, modified Broyden, and Anderson methods share common and key features, i.e. they all can be considered as quasi-Newton methods that try to minimize the residual/gradient norm with an explicit/implicit update of the inverse Hessian. In theory, DIIS is a quasi-Newton method that does not require explicit inverse Hessian information<sup>51</sup> and it also minimizes the residual norm via solving a set of linear equations. Hence, although empirical weight coefficients are required when updating new density/density matrix, modified Broyden and Anderson methods, as implemented in Paderborn DFTB code,<sup>26</sup> have comparable performance with DIIS, as is evident

by the results below.

For transition-metal compounds, near-degeneracies are often observed, which leads to difficulties in SCF convergence. This issue can be resolved via a Fermi temperature technique,<sup>59,60</sup> in which the occupation of orbitals is determined by a Fermi-Dirac distribution and the Fermi energy is set to be the middle point value between the highest occupied orbital (HOMO) and the lowest unoccupied molecular orbital (LUMO). The initially preset Fermi temperature is linearly decreased to 0 K or after the DIIS error is lower than a preset threshold value, which guarantees that the converged orbitals have integer occupancy. This technique has significantly improved the SCF convergence of many transition metal compound calculations,<sup>59,60</sup> although it does not guarantee convergence. On the other hand, for modified Broyden method and Anderson method, as implemented in Paderborn DFTB code, the orbitals with an energy difference of less than  $10^{-4}$  hartree are given the same (fractional) number of electrons. This is equivalent to a dynamical Fermi temperature-like technique and it often leads to converged SCF. However, the resultant wavefunction is not of single-determinant nature when the SCF converges to fractionally occupied orbitals. In fact, the wavefunction with fractionally occupied orbitals can be considered a multi-reference wavefunction.<sup>61</sup> However, such a dynamically fractionally occupied orbital approach is undesirable as it is unknown *a priori* whether the converged wavefunction has integer or fractional occupied orbitals, while also its multi-reference nature is not clearly defined.

**Geometry optimization.** Mathematically, the SCF procedure, i.e. wavefunction optimization, is a constrained optimization (due to MO orthogonality requirement) whereas geometry optimization is an unconstrained optimization provided no external geometry constraints are required. Regardless of this difference, some algorithms employed in SCF procedure can be directly applied to geometry optimization. For example, the DIIS algorithm is frequently applied in geometry optimization and is often referred to as GDIIS. One of the most robust optimization algorithms is the Broyden algorithm as used in the Gaussian program.<sup>45</sup> The Broyden algorithm is a rank- $m$  update of the Hessian matrix. The  $m$ -dimensional vector space is

spanned by the increments  $\Delta q$ , i.e. the geometry change at every step. These increment vectors are orthogonalized and thus result in an orthonormal vector basis. The Broyden algorithm is numerically stable and efficient in terms of computational time and required memory size. An alternative is the conjugate gradient method (CG), which has been implemented in the Paderborn DFTB code<sup>26</sup> and many other numerical optimization packages. CG can find a local minimal point along one dimension at every search step while maintaining the conjugacy between the current search direction and all previous ones. In addition, CG only requires two previous vectors to be stored. These numerically desirable properties make CG one of the most general and reliable optimization techniques in many areas.<sup>57,62</sup>

### **C. ONIOM approach: Employing the DFTB method as a polarizable buffer in multi-layer ONIOM**

Polarization effects play an important role in many chemical reactions. In many modern QM/MM approaches, the effects of polarization of the environment by the QM part can be included via a polarizable MM force field. Although, the past decade has seen significant progress in polarizable force field development,<sup>63-67</sup> their application is not always without problems or reliable.<sup>68-70</sup> Alternatively, compared with the use of a MM force field, it is often simpler and more effective to describe the effects of polarization of the environment by using a semiempirical method (SEQM) for a selected part of the environment.

While semiempirical methods are attractive as a low level method in ONIOM schemes since polarization effects and charge-transfer effects are naturally included, their computational cost is about 3 orders of magnitude larger than the traditional molecular mechanics method, which prohibits the application of a semiempirical method at the lowest level for a very large system. A reasonable compromise is to apply a three-layer ONIOM method, i.e. QM:SEQM:MM, where QM represents an appropriately selected high-level quantum mechanical method that can accurately describe the targeted chemical reactions; SEQM is a chosen semiempirical method that naturally includes polarization and charge-transfer effects; MM represents a molecular

mechanics method. In such a combination, the QM and SEQM regions can cover a large region, and problems related to the close proximity of the active region with the MM boundary will be alleviated or removed. The three-layer scheme has been proposed and tested using the DFT:AM1:Amber combination.<sup>71</sup>

Apart from the inclusion of the polarization effects between the QM region and the environment, using an ONIOM(QM:SEQM:MM) approach also allows for a simpler geometry optimization scheme than either QM/MM with a polarizable force field or ONIOM(QM:MM) or QM/MM with electronic embedding.<sup>72,73</sup>

To summarize section 2, we want to stress our density matrix-based formalism for one and two electron matrices as well as the Fock matrix. The implementation can make use of the same approaches for wave function optimization as for other *ab initio* methods implemented in the Gaussian package, as well as geometry optimizations. Some important new features in more details are:

a. The current implementation allows the construct of a new two-electron matrix to update the Fock matrix at every SCF iteration. During the update, direct SCF and differential Fock builder techniques by Almlöf *et al.*<sup>74</sup> can be used in the DFTB code, which is often computationally efficient for the optimization of large systems with hundreds or more atoms.

b. All wavefunction optimization techniques, e.g. EDIIS, CDIIS, damping, QC, are applicable to the DFTB method, which help SCF convergence and reduce computational cost in practice.

c. The geometry scan or optimization functions are readily available for the DFTB method to explore potential energy surface and investigate chemical reaction mechanisms, e.g. activation barrier calculations.

d. With the combination of other methods in ONIOM scheme, the DFTB method can be used in a wide range of applications, e.g. enzymatic catalysis.

e. In the context of *ab initio* molecular dynamics, the DFTB method can use the ADMP (atomic centered density matrix propagation) model for dynamics in many large systems that is

computationally prohibitive for DFT methods.<sup>75-77</sup>

f. The wavefunction symmetry and geometric symmetries can be fully exploited.

### 3. Computational details

All B3LYP/(SDD+6-31G(d)), PBE/PBE/(SDD+6-31G(d))<sup>78</sup> and CCSD(T)/(SDD+6-31G(d)) calculations are carried out using the Gaussian F.02 development program. (SDD+6-31G(d)) represents that the SDD basis set is applied to metal atoms while the 6-31G(d) basis set is applied to all other atoms. To test the difference in performance between the Gaussian and Paderborn implementation, we used both codes and optimized ten metallocene compounds including nickelocene, cobaltocene, ferrocene, scandocene, and titanocene molecules.<sup>26</sup> Both staggered and eclipsed conformers are included. In addition, two different spin states (three for iron) are computed for each compound for energy comparison. For SCF and geometry optimization performance calculations, the SCF convergence threshold is  $10^{-10}$  hartree in energy difference between successive iterations while the geometry was considered optimized if the maximal force component is less than 0.00045 a.u. A maximum number of 71 SCF cycles were performed at each geometry step, and geometry optimizations continued even if convergence had not been reached after the maximum number of SCF cycles. All ONIOM calculations were done using the Gaussian program with default criteria for SCF and geometry optimization.<sup>45</sup>

## 4. Results and Discussions

### A. SCF and geometry optimization convergence

In Figure 1, the average number of SCF iterations at every geometry step is shown, for the 10 metallocene compounds with two or three different spin states for each compound.<sup>b</sup> From this figure, it can be seen that for 14 out of a total of 22 compounds and states, the EDIIS + DIIS

---

<sup>b</sup> The numbers presented here are for illustrative purposes only; several other factors that affect the performance, such as initial guess, are different between the two implementations as well. However, these effects are small (at most a few cycles for each optimization) compared to the differences resulting from the DIIS and Broyden/Anderson approaches.

algorithm combined with Fermi temperature and damping technique requires the fewest number of iterations. This is due to the interpolation nature of EDIIS, which samples a wide range of the energy space at initial iterations and hence leads to faster convergence at later iterations. The second observation is that the Andersen method leads to faster convergence than the modified Broyden method, but the stability and general convergence properties of these methods are similar.<sup>58</sup> However, in 6 out of 22 compounds, EDIIS+DIIS in fact converges slower than the other two methods. The most problematic cases in DIIS are those involving iron triplet and quintet states. The frontier orbitals of the metallocenes in the initial staggered ( $D_{5d}$ ) and eclipsed ( $D_{5h}$ ) geometries increase their energies in the order:  $(d_{xy}, d_{(x^2-y^2)}) \sim (d_{z^2}) < (d_{xz}, d_{yz})$ .  $Fe^{2+}$  has a  $d^6$  configuration and the quintet state has three electrons in the degenerate  $d_{xy}$  and  $d_{(x^2-y^2)}$  orbitals, while the triplet has one electron in the degenerate  $d_{xz}$  and  $d_{yz}$  orbitals. In the present calculations, the doubly degenerate electronic configuration in each case lead to difficult SCF convergence for some geometries during the optimization. The modified Broyden method and Anderson method as implemented in Paderborn DFTB code allow fractional occupancy, i.e. assigning same (fractional) number of electrons into orbitals with energy difference less than  $10^{-4}$  hartree, which provide better orbitals on the fly, and results in a better convergence performance. But one unfavorable effect is that such wavefunction with fractional occupancy is a configuration average of several determinants,<sup>61</sup> whose physical meaning is clear in *ab initio* theory while rather vague in an approximate density-functional theory context. In addition, such fractional occupancy is not under strict control, i.e. when it happens is not known *a priori*. This adds arbitrariness into the final result. Given the fact that all SCFs in our calculations can be converged, the EDIIS+DIIS algorithm is more desirable from our point of view.

In geometry optimization, the Bery algorithm uses less than 20 steps for geometry optimization for all 22 compounds shown in Figure 2, while the conventional CG method often converges in more than 20 steps. Figure 2 clearly indicates the superiority of the Bery algorithm over the CG method.

## **B. Performance of the DFTB method in geometry and spin splitting energy of ferrocene, cobaltocene, and nickelocene**

In this section, PBEPBE refers to PBEPBE/(SDD+6-31G(d)), B3LYP refers to B3LYP/(SDD+6-31G(d)), and CCSD(T) refers to CCSD(T)/(SDD+6-31G(d)). Because the comparison is between high-level methods and the DFTB method, which has been parameterized against DFT results with double-zeta basis set, the use of a small basis sets is justified. The energies of ferrocene, cobaltocene, and nickelocene are taken from the eclipsed conformers. The energy differences between staggered and eclipsed conformers are very small (<0.1 kcal/mol for DFTB calculations); selecting only the eclipsed conformers for benchmark tests should therefore has a very small effect on the reported results. As shown in Figure 3, compared to experimental values,<sup>79,80</sup> both PBEPBE and B3LYP methods give good optimized distances, consistent with many previous benchmark results.<sup>81-84</sup> Although the results are not converged with regard to the basis set, the deviation of the metal-carbon bond length is less than 0.05Å for both PBEPBE and B3LYP results in comparison to experimental values. In contrast, in the DFTB method the metal carbon length is about 0.2 Å longer than the experimental value for ferrocene and nickelocene although the deviation is much smaller for cobaltocene. Such geometry performance is also observed in our previous paper,<sup>25</sup> and may be further improved by refining the currently used parameters.

In Figure 4, we plot the spin splitting energy for staggered conformers of ferrocene, cobaltocene and nickelocene. The spin splitting energy here is defined as ( $E_{\text{high\_spin}} - E_{\text{low\_spin}}$ ). For ferrocene and nickelocene, the spin states are singlet and triplet, while for cobaltocene they are doublet and quartet. Experimentally, based on measured magnetic moments,<sup>79,80</sup> ferrocene has a singlet ground state, cobaltocene is a doublet and nickelocene is a triplet. Results from CCSD(T), which is based on PBEPBE optimized geometry, give the correct spin-state assignment. From Figure 4, both PBEPBE and DFTB method reproduce the experimental energy order between low-spin and high-spin state. The stability of high-spin species increases in the series Fe, Co, and Ni as calculated by CCSD(T), PBEPBE and B3LYP.<sup>78</sup> For cobaltocene,

B3LYP predicts the quartet state to be more stable than the doublet state by a small margin. The spin-state assignment may change with the use of another basis set, but the results are consistent with observations that the B3LYP functional favors high-spin states due to the inclusion of 20 % exact exchange.<sup>83,84</sup> In contrast, the increasing trend of high spin state in Fe, Co, and Ni series is not reproduced by the DFTB method, which is known from our previous investigations.<sup>25</sup>

### **C. Application and performance test for single-walled carbon nanotube (SWCNT) molecule**

The geometry performance of the DFTB method for organic compounds, especially for fullerene and carbon nanotubes, has been extensively tested by us<sup>24</sup> and other groups.<sup>8,11,85</sup> We have shown that the DFTB method can accurately calculate the geometries of fullerene molecules and the relative energy order of a set of fullerene isomers, compared to DFT calculations.<sup>24</sup> In addition, we have successfully employed the DFTB method to study fullerene and carbon nanotube molecule formation using quantum mechanical/molecular dynamics method and also to study the surface chemistry of carbon nanotubes.<sup>36-41,86</sup>

Here, we further test the performance of the DFTB method using the new DFTB implementation on the geometry and HOMO and LUMO energies of (5,5)-SWCNT of different lengths. The systems are  $C_{10n}H_{20}$ , in which  $n$  represents the number of layers surrounding the tube axis, with  $C_{50}H_{20}$  for  $n=5$  as the shortest and  $C_{150}H_{20}$  for  $n=15$  as the longest. Geometries are fully optimized at the SCC-DFTB and B3LYP/6-31G(d) level<sup>84</sup> with full exploitation of the symmetry. The default convergence criterion for SCF is adopted; the SCF is considered converged only when changes in both density matrix elements and total energy between consecutive iterations are smaller than the default threshold values.

In Table 1, geometrical differences between SCC-DFTB and B3LYP/6-31G(d) optimized structures of (5,5) SWCNT of different lengths are shown. In these calculations, the full molecular structural symmetry is used; (5,5)-SWCNT ( $C_{10n}H_{20}$ ) has  $D_{5d}$  and  $D_{5h}$  symmetry when  $n$  is even and odd number, respectively. Of all bond lengths, the maximum bond length

difference is about 0.014 Å except for the molecule with  $n=12$  where the maximum bond length difference is 0.025 Å. The root mean square (RMS) bond length difference is about 0.007 Å excluding 0.013 Å for  $n=12$ . In line with the bond length performance, the maximum bond angle differences of these SWCNT molecules are all less than 1.0 degree and the RMS difference is about 0.35 degree. These observations are consistent with those obtained previously by our group and others.<sup>8,11,24</sup> In summary, the present test shows that the DFTB method can accurately predict the SWCNT molecular structures compared with those at the B3LYP/6-31G(d) level.

Both DFTB HOMO and LUMO energies of these SWCNT, indicators of reactivity toward the nucleophilic and electrophilic attacks,<sup>87</sup> shown in Figure 5, are parallel to the B3LYP/6-31G(d) results. Especially, the HOMO energy difference between the DFTB method and B3LYP/6-31G(d) is rather small and is almost constant among all these molecules. This is what is expected and is consistent to performance of the DFTB method for ionization potentials found by Thiel et al.,<sup>8</sup> as the HOMO energy is the negative of ionization potential in Kohn-Sham DFT theory and the DFTB method has been parameterized to mimic B3LYP/6-31G(d) energies. Although the LUMO energy difference between the DFTB method and B3LYP/6-31G(d) among all these molecules is almost constant, the difference in the absolute energy of LUMO is much larger than that in HOMO. This large deviation in LUMO energy is due to the known basis set effect, for which only valence minimal basis set is adopted in the DFTB method.<sup>88</sup>

As shown in Figure 5, both the HOMO and the LUMO energies in both the DFTB and B3LYP/6-31G(d) methods change with the periodicity is 3 as the number of layers ( $n$ ) in (5,5) SWCNT increases sequentially. As pointed out by Nakamura et al.,<sup>89</sup> this pattern comes from the fact that as the number  $n$  increases in (5,5) SWCNT  $C_{10n}H_{20}$ , the molecules will assume a Kekulé structure (e.g.  $n=4$ ,  $C_{40}H_{20}$ ), incomplete Clar structure (e.g.  $n=5$ ,  $C_{50}H_{20}$ ) and complete Clar structure (e.g.  $n=6$ ,  $C_{60}H_{20}$ ) with a periodicity of 3. Furthermore, the DFTB method results exactly predict the HOMO and LUMO energy change pattern among three different types of structures as well as the HOMO-LUMO energy gaps. These indicate that the DFTB method reproduces the different reactivity of carbon nanotube molecules with respect to the increase of

tube lengths.

#### **D. ONIOM method with the DFTB method**

To illustrate the benefits of a DFTB layer in the ONIOM method, we calculated the reaction energy of a proton transfer between two histidines, a reaction where the effect of charge-transfer and polarization due to the surrounding amino acids is expected to be important. The five-residue system we studied, shown in Fig. 6, does not represent any specific protein site; instead it is designed to maximize the residue effects of polarization and provide a stringent test of the capabilities of the DFTB method as the polarizable middle layer in three-layer ONIOM (QM:SEQM:MM) calculations.

Reference proton transfer energies are evaluated at the B3LYP/6-31G(d) level, because this is the basis set level for which the DFTB method has been parameterized. In the QM:MM calculations, the Amber96 force field has been used for the MM region.<sup>90</sup> Residue models are truncated at the C<sub>α</sub>-C<sub>β</sub> bond and the MM charge of the C<sub>β</sub> atom has been adjusted to achieve integral residue charges. The lack of protein framework exaggerates the mobility of the residues, and to ensure comparisons between the same local minima, model geometries optimized at the B3LYP/6-31G(d) level are used throughout. Moving the proton from the (polarized) histidine (His2) to the (unpolarized) histidine (His1) is an endothermic process without barrier. To be able to calculate the energy of both states, the respective N-H bond distance is frozen at 1.05 Å in both reactant and product.

Reaction energies for different models and ONIOM divisions are given in Table 2. It is illustrative to first look at the three-residue model where aspartate is the single polarizing residue (model B). At the reference B3LYP/6-31G(d) level (system B.1 in Table 2), the proton transfer energy is 22.7 kcal/mol, i.e., the aspartate increases the relative proton affinity of the neighboring histidine by 22.7 kcal/mol. The value is very similar (22.5 kcal/mol) at the PBEPBE/6-31G(d) level, and drops by a few kcal/mol (to 20.3 kcal/mol) with B3LYP/6-311++G(2df,2pd). Using the DFTB method to describe the aspartate in an

ONIOM(DFT:DFTB) model (system B.2), gives a reaction energy of 23.9 kcal/mol, see Fig. 7. The deviation compared to the reference B3LYP/6-31G(d) value is 1.2 kcal/mol, only 5 % of the total effect.

The ONIOM(DFT:DFTB) results are favorably compared to results from the ONIOM (DFT:MM) method. With ONIOM (DFT:MM-EE) (electronic embedding, system B.3) the reaction energy is 16.4 kcal/mol and the deviation compared to full DFT is 6.3 kcal/mol. Applying ONIOM(DFT:MM-ME) (mechanical embedding with classical evaluation of electrostatics based on the updated ESP charges of the model QM part, system B.4) gives a result of 15.5 kcal/mol, rather similar to electronic embedding. However, if mechanical embedding is applied using the original Amber charges without reparameterizing (system B.5), a large part of the electrostatic effect is neglected and the reaction energy is severely underestimated. The reason why all ONIOM(DFT:MM) methods underestimate the effect of the aspartate is likely due to the neglect of charge transfer. It should also be noted that the ONIOM(DFT:DFTB) system also performs better than full DFTB (system B.6), where the deviation from the target DFT result is 4.6 kcal/mol.

Adding a positively charged lysine residue (Model C) decreases the proton affinity of His2 and the target reaction energy becomes 11.0 kcal/mol with full DFT (system C.1). The DFTB method describes the effect of the lysine within 1 kcal/mol (system C.2), but if both aspartate and lysine are described by DFTB (system C.3), the errors add up and the total deviation is 2.4 kcal/mol. Including both aspartate and lysine at the MM level gives small deviations (0.1 kcal/mol with electronic embedding and 2.4 kcal/mol with mechanical embedding and updated charges), but this is likely due to cancellation of errors.

Finally, adding a serine to represent neutral residues included in the hydrogen bond network (model D), gives a proton transfer energy of 11.5 kcal/mol with full DFT (system D.1). The effect of the serine is rather small (0.2–0.6 kcal/mol) at all levels of theory, see Table 2, and this type of residue can be included in the cheap MM layer. A balanced ONIOM treatment of the five-residue system is thus to describe the reacting histidines with DFT, the polarizing aspartate

and lysine residues with the DFTB method, and the neutral serine residue with MM (system D.5), see Figure 6. For this ONIOM (DFT:DFTB:MM-ME) system, the reaction energy is 14.2 kcal/mol, a deviation from the full DFT result of 2.7 kcal/mol.

The present example illustrates the use of the DFTB method as a low-level QM method in ONIOM calculations and shows that ONIOM(DFT:DFTB) method can describe large polarization effects with reasonable accuracy. In real proteins, the number of contributing residues is much larger and the size of the respective QM and SEQM layers should be increased to reduce errors from individual residues. In ONIOM(DFT:DFTB) models, the polarization effect is fully described at the DFTB level. To get reasonable results, the change in charge distribution during the reaction must be described similarly by both DFT and the DFTB method. Further tests of the accuracy of ONIOM(DFT:DFTB) models for a wider range of reactions will be performed in later studies.

#### **4. Conclusions**

In this article, we present theoretical and implementation details of the DFTB method into the Gaussian package. Benchmark tests of the DFTB method using this code on SWCNT molecules are also presented, and they clearly show that the DFTB method can reproduce the results at B3LYP level well. These results are consistent with our previous tests and also promise the DFTB method to be a very favorable method in a wide range of applications, including material science and biomolecular reactions.

In addition, the performance of the default algorithms for SCF and geometry optimization in the Gaussian program is very encouraging compared with other methods. These algorithms play important roles in practical calculations, especially for large systems. Also, it makes possible to apply the DFTB method to larger system sizes.

Third, benchmark calculations including the DFTB method in ONIOM method have clearly shown the promise of employing ONIOM in biomolecular systems. More importantly, the description of polarization effect by the DFTB method opens up opportunities for many

applications using the three-layer ONIOM method.

### **Acknowledgements**

Authors are grateful for many useful discussions with Drs. Marcus Elstner, Henryk A. Witek, Thomas Frauenheim, Thomas Köhler and Gotthard Seifert. Acknowledgements are also made to Drs. Petia Bobadova-Parvanova, Rajeev Prabhakar and Stephan Irle as well as Yoko Sasakura, Zhi Wang, Dr. Lung-Wa Chung, and Dr. Baoshan Wang for many helpful tests during the DFTB code implementation. M.L. acknowledges the Fukui Institute Fellowship. The present research is in part supported by Japan Science and Technology Agency (JST) with a Core Research for Evolutional Science and Technology (CREST) grant in the Area of High Performance Computing for Multiscale and Multiphysics Phenomena and also in part by a grant to Emory University from Gaussian, Inc. The computational resource at Research Center of Computer Science (RCCS) at the Institute for Molecular Science (IMS) is also acknowledged.

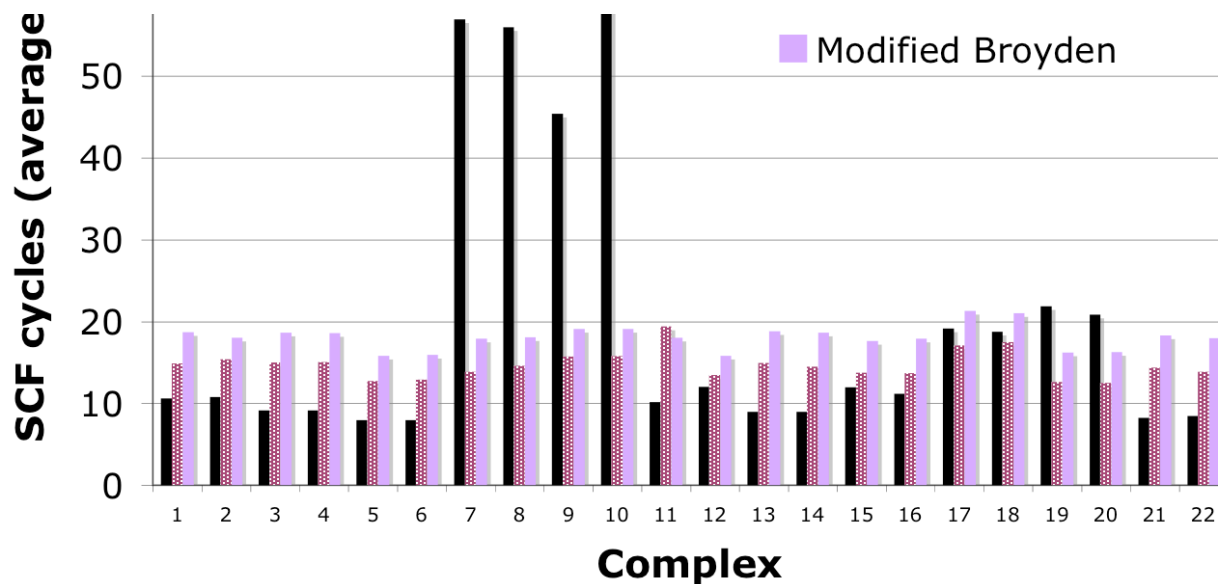


Figure 1. The average SCF iteration number per geometry step for metallocenes, i.e.  $\text{Co}(\text{C}_5\text{H}_5)_2$  (1: eclipse doublet; 2: stagger doublet; 3: eclipse quartet; 4: stagger quartet),  $\text{Fe}(\text{C}_5\text{H}_5)_2$  (5: eclipse singlet; 6: stagger singlet; 7: eclipse triplet; 8: stagger triplet; 9: eclipse quintet; 10: stagger quintet),  $\text{Ni}(\text{C}_5\text{H}_5)_2$  (11: eclipse singlet; 12: stagger singlet; 13: eclipse triplet; 14: stagger triplet),  $\text{Sc}(\text{C}_5\text{H}_5)_2$  (15: eclipse doublet; 16: stagger doublet; 17: eclipse quartet; 18: stagger quartet),  $\text{Ti}(\text{C}_5\text{H}_5)_2$  (19: eclipse singlet; 20: stagger singlet; 21: eclipse triplet; 22: stagger triplet).

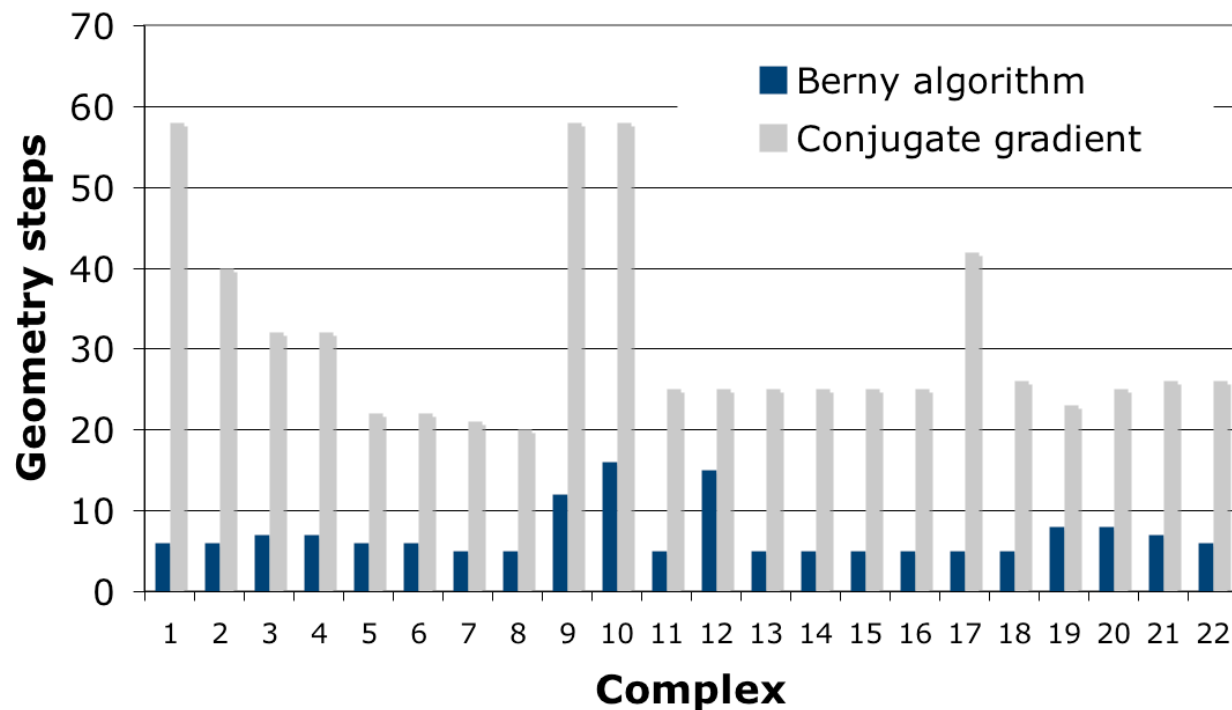


Figure 2. The number of geometry optimization steps. Berny algorithm is used in Gaussian DFTB code while conjugate gradient method is used in Paderborn DFTB code. The complex numbering is the same as in Figure 1.

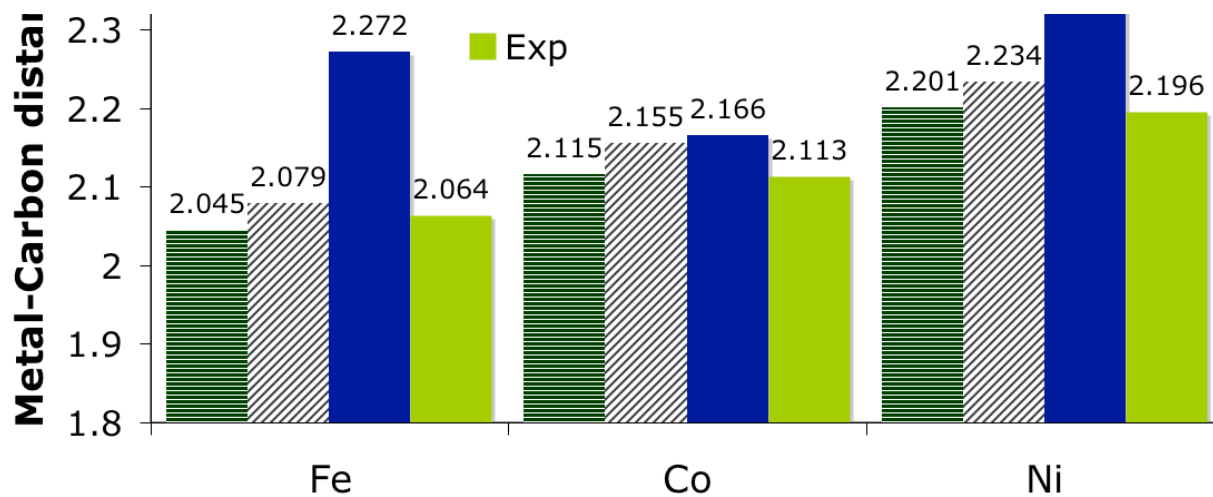


Figure 3. The average metal carbon distance computed with PBE/PBE/(SDD+6-31G(d)), B3LYP/(SDD+6-31G(d)), and the DFTB method. The spin state for ferrocene, cobaltocene, and nickelocene is singlet, doublet, and triplet, respectively. Experimental values are also given for reference.<sup>79,80</sup>

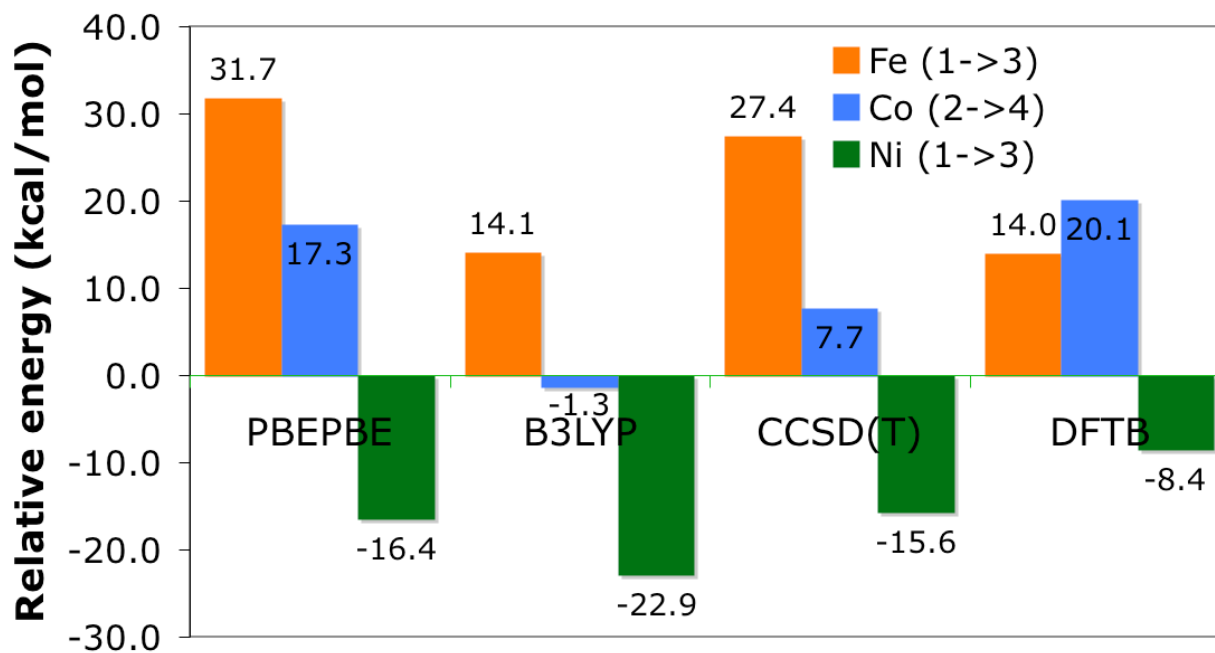


Figure 4. The spin splitting energy (high\_spin – low\_spin) for eclipse ferrocene, cobaltocene and nickelocene at PBEPBE/(SDD+6-31G(d)), B3LYP/(SDD+6-31G(d)), CCSD(T)/(SDD+6-31G(d)), and DFTB methods. The energy value of CCSD(T)/(SDD+6-31G(d)) is based on PBEPBE/(SDD+6-31G(d)) optimized geometry.

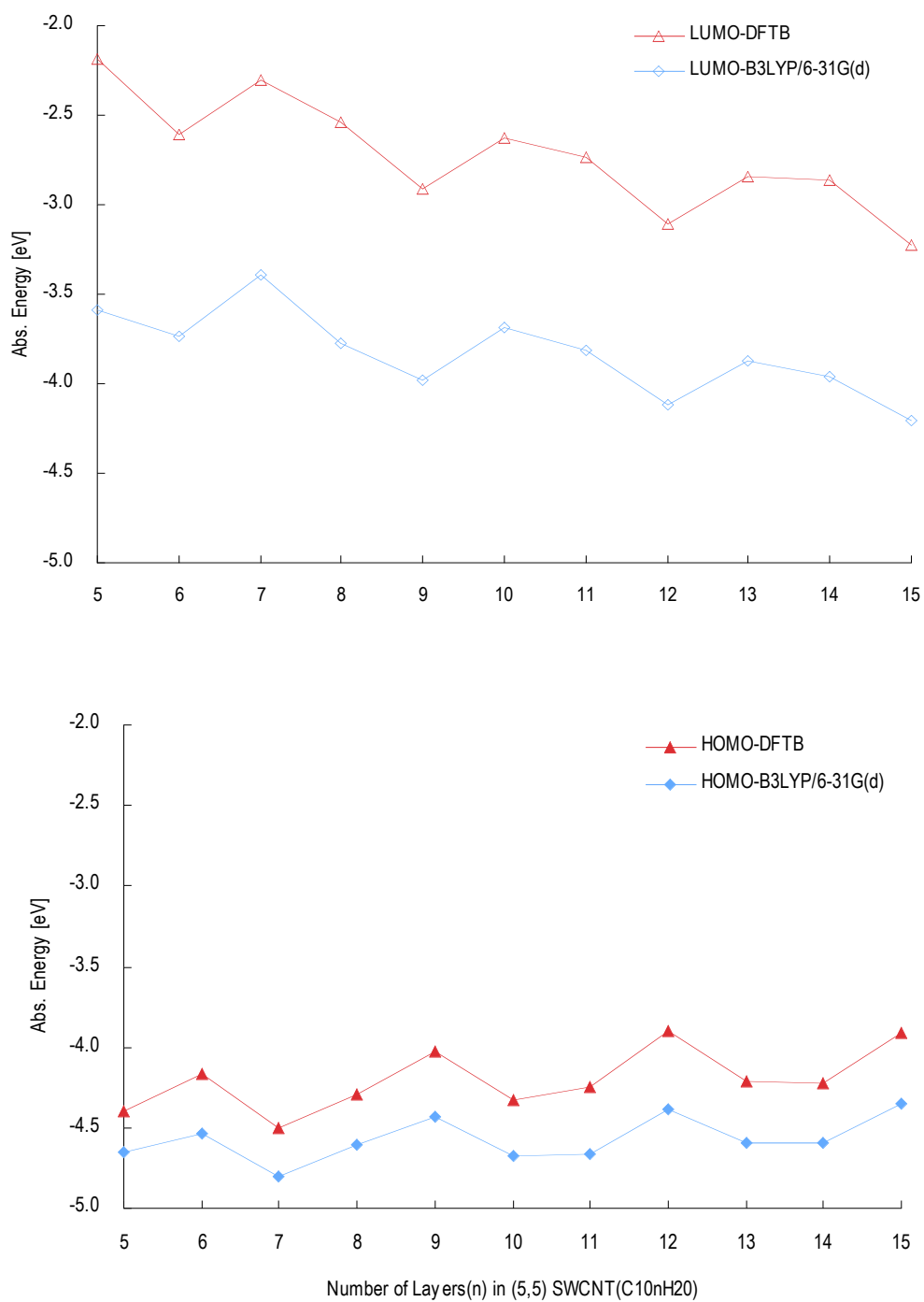


Figure 5. HOMO and LUMO energies of the finite length (5,5) SWCNT( $C_{10n}H_{20}$ ). The values are determined by the DFTB method and B3LYP/6-31G(d).

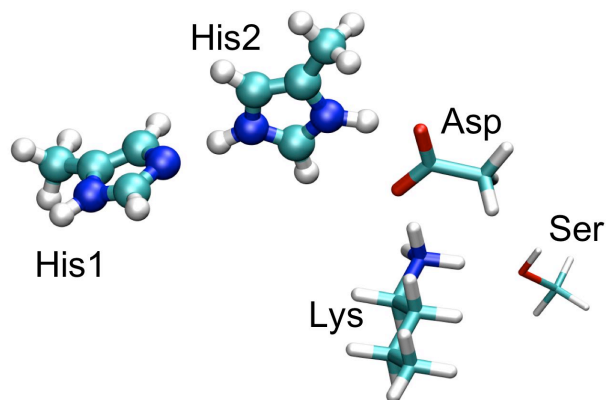


Figure 6. Five-residue system used in ONIOM investigations. Model A includes the histidine residues, model B additionally includes the aspartate, and model C also the lysine. Finally, model D represents the full system. The illustration is made for a three-layer ONIOM(DFT:DFTB:MM) system with the model (reactive) system in ball and stick, the intermediate (polarizing) system in stick representation, and the real system in thin stick representation (system D.6).

Table 1. The geometrical parameter difference of (5,5) SWCNT ( $C_{10n}H_{20}$ ) determined by DFTB and B3LYP/6-31G(d). The maximum and root mean square differences are denoted by Max and RMS. All bond lengths and angles are compared.

# of layer (n)	Bond Length Diff. [Å]		Bond Angle Diff. [deg]	
	Max	RMS	Max	RMS
5	0.014	0.008	0.63	0.30
6	0.014	0.008	0.72	0.35
7	0.013	0.007	0.70	0.33
8	0.014	0.007	0.72	0.31
9	0.014	0.007	0.70	0.31
10	0.014	0.007	0.64	0.27
11	0.013	0.006	0.68	0.26
12	0.025	0.013	0.92	0.34
13	0.014	0.006	0.64	0.25
14	0.013	0.006	0.67	0.24
15	0.013	0.006	0.68	0.25

Table 2. Relative energy of a proton transfer from a polarized histidine (His2) to an unpolarized histidine (His1). The DFT method is B3LYP/6-31G(d) and the MM force field is Amber96. MM-EE is electronic embedding, MM-ME(ESP) is mechanical embedding with model charges updated from ESP calculations, and MM-ME is mechanical embedding where the original Amber charges are used for both reactant and product.

System	His1	His2	Asp	Lys	Ser	Reaction energy (kcal/mol)
A.1	DFT	DFT	-	-	-	0.0
B.1	DFT	DFT	DFT	-	-	22.7
B.2	DFT	DFT	DFTB	-	-	23.9
B.3	DFT	DFT	MM-EE	-	-	16.4
B.4	DFT	DFT	MM-ME(ESP)	-	-	15.5
B.5	DFT	DFT	MM-ME	-	-	3.1
B.6	DFTB	DFTB	DFTB	-	-	27.3
C.1	DFT	DFT	DFT	DFT	-	11.0
C.2	DFT	DFT	DFT	DFTB	-	12.0
C.3	DFT	DFT	DFTB	DFTB	-	13.4
C.4	DFT	DFT	MM-EE	MM-EE	-	11.1
C.5	DFT	DFT	MM-ME(ESP)	MM-ME(ESP)	-	13.6
C.6	DFT	DFT	MM-ME	MM-ME	-	3.0
C.7	DFTB	DFTB	DFTB	DFTB	-	15.3
D.1	DFT	DFT	DFT	DFT	DFT	11.5
D.2	DFT	DFT	DFT	DFT	DFTB	11.6
D.3	DFT	DFT	DFT	DFT	MM-ME	11.2
D.4	DFT	DFT	DFTB	DFTB	DFTB	14.6
D.5	DFT	DFT	DFTB	DFTB	MM-ME	14.2
D.6	DFT	DFT	MM-EE	MM-EE	MM-EE	10.1

## References.

1. Parr, R. G.; Yang, W. *Density-Functional Theory of Atoms and Molecules*; Oxford University Press: New York, 1989.
2. Dewar, M. J. S.; Jie, C.; Yu, J. *Tetrahedron* 1993, 49, 5003-5038.
3. Dewar, M. J. S.; Thiel, W. J. *Am. Chem. Soc.* 1977, 99, 4899-4907.
4. Dewar, M. J. S.; Thiel, W. J. *Am. Chem. Soc.* 1977, 99, 4907-4917.
5. Dewar, M. J. S.; Zoebisch, E.; Healy, E. F.; Stewart, J. J. P. *J. Am. Chem. Soc.* 1985, 107, 3902-3909.
6. Thiel, W.; Voityuk, A. A. *Theor. Chim. Acta* 1992, 81, 391-404.
7. Thiel, W.; Voityuk, A. A. *Theor. Chim. Acta* 1996, 93, 315-315.
8. Otte, N.; Scholten, M.; Thiel, W. *J. Phys.Chem.A* 2007, 111, 5751-5755.
9. Weber, W.; Thiel, W. *Theor. Chem. Acc.* 2000, 103, 495-506.
10. Repasky, M. P.; Chandrasekhar, J.; Jorgensen, W. *J. Comput. Chem.* 2002, 23, 1601-1622.
11. Sattlemeyer, K. W.; Tirado-Rives, J.; Jorgensen, W. L. *J. Phys.Chem.A* 2006, 110, 13551-13559.
12. Sattlemeyer, K. W.; Tubert-Brohman, I.; Jorgensen, W. L. *J. Chem. Theory Comput.* 2006, 2, 413-419.
13. Stewart, J. J. P. *J. Comput. Chem.* 1989, 10, 209-220.
14. Rocha, G. B.; Freire, R. O.; Simas, A. M.; Stewart, J. J. P. *J. Comput. Chem.* 2006, 27, 1101-1111.
15. Nanda, D. N.; Jug, K. *Theor. Chim. Acta* 1980, 57, 95-106.
16. Jug, K.; Iert, R.; Schulz, J. *Int. J. Quantum Chem.* 1987, 32, 265-277.
17. Li, J.; Mello, P. C. d.; Jug, K. *J. Comput. Chem.* 1992, 13, 85-92.
18. Bredow, T.; Geudtner, G.; Jug, K. *J. Comput. Chem.* 2001, 22, 861-887.
19. Bredow, T.; Jug, K. *Theor. Chem. Acc.* 2005, 113, 1-14.
20. Ahlswede, B.; Jug, K. *J. Comput. Chem.* 1999, 20, 563-571.
21. Witek, H. A.; Irle, S.; Morokuma, K. *J. Chem. Phys.* 2004, 121, 5163-5170.
22. Witek, H. A.; Morokuma, K. *J. Comput. Chem.* 2004, 25, 1858 - 1864.
23. Witek, H. A.; Morokuma, K.; Stradomska, A. *J. Chem. Phys.* 2004, 121, 5171-5178.
24. Zheng, G.; Irle, S.; Morokuma, K. *Chem. Phys. Lett.* 2005, 412, 210-216.
25. Zheng, G.; Witek, H.; Bobadova-Parvanova, P.; Irle, S.; Musaeu, D. G.; Prabhakar, R.; Morokuma, K.; Lundberg, M.; Elstner, M.; Kohler, C.; Frauenheim, T. *J. Chem. Theory Comput.* 2007, 3, 1349-1367.
26. Porezag, D.; Frauenheim, T.; Köhler, T.; Seifert, G.; Kaschner, R. *Phys. Rev. B* 1995, 51, 12947-12957.
27. Elstner, M.; Porezag, D.; Jungnickel, G.; Elsner, J.; Haugk, M.; Frauenheim, T.; Suhai, S.; Seifert, G. *Phys. Rev. B* 1998, 58, 7260-7268.
28. Köhler, C.; Seifert, G.; Gerstmann, U.; Elstner, M.; Overhof, H.; Frauenheim, T. *Phys. Chem. Chem. Phys.* 2001, 3, 5109-5114.
29. Kolb, M.; Thiel, W. *J. Comput. Chem.* 1993, 14, 775-789.
30. Morokuma, K. *Bull. Korean Chem. Soc.* 2003, 24, 797-801.
31. Svensson, M.; Humbel, S.; Froese, R. D. J.; Matsubara, T.; Sieber, S.; Morokuma, K. *J. Phys. Chem.* 1996, 100, 19357-19363.
32. Humbel, S.; Sieber, S.; Morokuma, K. *J. Chem. Phys.* 1996, 105, 1959-1967.
33. Field, M. J.; Bash, P. A.; Karplus, M. *J. J. Comput. Chem.* 1990, 11, 700-733.
34. Warshel, A.; Levitt, M. *J. Mol. Biol.* 1976, 103, 227-249.
35. Wang, I. S. Y.; Karplus, M. *J. Am. Chem. Soc.* 1973, 95, 8160-8164.

36. Zheng, G.; Irle, S.; Elstner, M.; Morokuma, K. *J. Phys. Chem. A* 2004, 108, 3128-3194.
37. Zheng, G.; Irle, S.; Morokuma, K. *J. Chem. Phys.* 2004, 122, 014708/014701-014708/014707.
38. Zheng, G.; Irle, S.; Morokuma, K. *J. Nanosci. Nanotechnol.* 2006, 6, 1259-1270.
39. Irle, S.; Zheng, G.; Elstner, M.; Morokuma, K. *Nano Lett.* 2003, 3, 465-470.
40. Irle, S.; Zheng, G.; Elstner, M.; Morokuma, K. *Nano Lett.* 2003, 3, 1657-1664.
41. Irle, S.; Zheng, G.; Elstner, M.; Morokuma, K. *Theory and Applications of Computational Chemistry: The First 40 Years*, Seoul, Korea, 2004.
42. Singh, U. C.; Kollman, P. A. *J. Comput. Chem.* 1986, 7, 718-730.
43. Frauenheim, T.; Seifert, G.; Elstner, M.; Hajnal, Z.; Jungnickel, G.; Porezag, D.; Suhai, S.; Scholz, R. *Phys. Status Solidi (b)* 2000, 217, 41-62.
44. Frauenheim, T.; Seifert, G.; Elstner, M.; Niehaus, T.; Kohler, C.; Amkreutz, M.; Sternberg, M.; Zoltan Hajnal; Carlo, A. D.; Suhai, S. *J. Phys-Condens Mat.* 2002, 14, 3015-3047.
45. Gaussian 03, Revision F.02, M. J. Frisch, G. W. Trucks, H. B. Schlegel, G. E. Scuseria, M. A. Robb, J. R. Cheeseman, J. A. Montgomery, Jr., T. Vreven, G. Scalmani, B. Mennucci, V. Barone, G. A. Petersson, M. Caricato, H. Nakatsuji, M. Hada, M. Ehara, K. Toyota, R. Fukuda, J. Hasegawa, M. Ishida, T. Nakajima, Y. Honda, O. Kitao, H. Nakai, X. Li, H. P. Hratchian, J. E. Peralta, A. F. Izmaylov, K. N. Kudin, J. J. Heyd, E. Brothers, V. Staroverov, G. Zheng, R. Kobayashi, J. Normand, J. L. Sonnenberg, S. S. Iyengar, J. Tomasi, M. Cossi, N. Rega, J. C. Burant, J. M. Millam, M. Klene, J. E. Knox, J. B. Cross, V. Bakken, C. Adamo, J. Jaramillo, R. Gomperts, R. E. Stratmann, O. Yazyev, A. J. Austin, R. Cammi, C. Pomelli, J. W. Ochterski, P. Y. Ayala, K. Morokuma, G. A. Voth, P. Salvador, J. J. Dannenberg, V. G. Zakrzewski, S. Dapprich, A. D. Daniels, M. C. Strain, O. Farkas, D. K. Malick, A. D. Rabuck, K. Raghavachari, J. B. Foresman, J. V. Ortiz, Q. Cui, A. G. Baboul, S. Clifford, J. Cioslowski, B. B. Stefanov, G. Liu, A. Liashenko, P. Piskorz, I. Komaromi, R. L. Martin, D. J. Fox, T. Keith, M. A. Al-Laham, C. Y. Peng, A. Nanayakkara, M. Challacombe, W. Chen, M. W. Wong, J. A. Pople. Gaussian Inc.: Wallingford CT, 2006.
46. Harris, J. *Phys.Rev.B* 1985, 31, 1770-1779.
47. Saunders, V. R.; Hillier, I. H. *Int. J. Quantum Chem.* 1973, 7, 699-705.
48. Mitin, A. V. *J. Comput. Chem.* 1988, 9, 107-110.
49. Francisco, J. B.; Martinez, J. M.; Martinez, L. *J. Chem. Phys.* 2004, 121, 10863-10878.
50. Thogersen, L.; Olsen, J.; Yeager, D.; Jorgensen, P.; Salek, P.; Helgaker, T. *J. Chem. Phys.* 2001, 121, 16-27.
51. Thogersen, L.; Olsen, J.; Kohn, A.; Jorgensen, P.; Salek, P.; Helgaker, T. *J. Chem. Phys.* 2005, 123, 074103
52. Hartree, D. R. *The Calculation of Atomic Structure*; Wiley, 1957.
53. Pulay, P. *Chem. Phys. Lett.* 1980, 73, 393-398.
54. Kudin, K. N.; Scuseria, G. E.; Cancés, E. *J. Chem. Phys.* 2002, 116, 8255-8261.
55. Bacskay, G. B. *Chem. Phys.* 1981, 61, 385-404.
56. Pulay, P. *J. Comp. Chem.* 1982, 3, 556.
57. Saad, Y. *Iterative Methods for Sparse Linear Systems*; SIAM: Philadelphia, 2003.
58. Eyert, V. *J. Comput. Phys.* 1996, 124, 271-285.
59. Rabuck, A. D.; Scuseria, G. E. *J. Chem. Phys.* 1999, 110, 478177.
60. Warren, R. W.; Dunlap, B. I. *Chem. Phys. Lett.* 1999, 262, 384-392.
61. McWeeny, R. *Methods of Molecular Quantum Mechanics*; Academic Press: San Diego, 1992.
62. Nocedal, J.; Wright, S. J. *Numerical Optimization*; Springer: New York, 1999.
63. Stern, H. A.; Kaminski, G. A.; Banks, J. L.; Zhou, R.; Berne, B. J.; Friesner, R. A. *J. Phys. Chem. B* 1999, 103,

4730-4737.

64. Banks, J. L.; Kaminski, G. A.; Zhou, R.; Mainz, D. T.; Berne, B. J.; Friesner, R. A. *J. Chem. Phys.* 1999, 110, 741.
65. Rappé, A. K.; Casewit, C. J.; Colwell, K. S.; W. A. Goddard, I.; Skiff, W. M. *J. Am. Chem. Soc.* 1992, 114, 10024.
66. Rappé, A. K.; Goddard, W. A. I. *J. Phys. Chem.* 1991, 95, 3358-3363.
67. Ponder, J. W.; Ren, P. J. *Phys. Chem. B* 2003, 107, 5933-5947.
68. Chen, J.; Martinez, T. J. *Chem. Phys. Lett.* 2007, 438, 315-320.
69. Morales, J.; Martinez, T. J. *J. Phys. Chem. A* 2004, 108, 3076-3084.
70. Morales, J.; Martinez, T. J. *J. Phys. Chem. A* 2001, 105, 2842-2850.
71. Morokuma, K.; Wang, Q.; Vreven, T. *J. Chem. Theor. Comput.* 2006, 2, 1317-1324.
72. Vreven, T.; Frisch, M. J.; Kudin, K. N.; Schlegel, H. B.; Morokuma, K. *Mol. Phys.* 2006, 104, 701-714.
73. Vreven, T.; Morokuma, K.; Farkas, Ö.; Schlegel, H. B.; Frisch, M. J. *J. Comput. Chem.* 2003, 24, 760-769.
74. Almlöf, J.; Faegri, K., Jr; Korsel, K. *J. Comput. Chem.* 1982, 3, 385.
75. Schlegel, H. B.; Iyengar, S. S.; Li, X.; Millam, J. M.; Voth, G. A.; Scuseria, G. E.; Frisch, M. J. *J. Chem. Phys.* 2002, 117, 8694.
76. Schlegel, H. B.; Millam, J. M.; Iyengar, S. S.; Voth, G. A.; Daniels, A. D.; Scuseria, G. E.; Frisch, M. J. *J. Chem. Phys.* 2001, 114, 9758.
77. Iyengar, S. S.; Schlegel, H. B.; Millam, J. M.; Voth, G. A.; Scuseria, G. E.; Frisch, M. J. *J. Chem. Phys.* 2001, 115, 10291.
78. Perdew, J. P.; Burke, K.; Ernzerhof, M. *Phys. Rev. Letts.* 1996, 77, 3865-3868.
79. Salomon, O.; Reiher, M.; Hess, B. A. *J. Chem. Phys.* 2002, 117, 4729-4737.
80. Holleman, A. F.; Wiberg, E.; Wiberg, N. *Lehrbuch der Anorganischen Chemie*; Walter de Gruyter: Berlin, 1995.
81. Sears, J. S.; Sherrill, C. D. *J. Phys. Chem. A* 2008, 112, 3466-2477.
82. Zhao, Y.; Truhlar, D. G. *J. Phys. Chem. A* 2004, 108, 6908-6918.
83. Stephens, P. J.; Devlin, F. J.; Chabalowski, C. F.; Frisch, M. J. *J. Phys. Chem.* 1994, 98, 11623-11627.
84. Becke, A. D. *J. Chem. Phys.* 1993, 98, 5648-5652.
85. Krüger, T.; Elstner, M.; Schiffels, P.; Frauenheim, T. *J. Chem. Phys.* 2005, 122, 114110.
86. Irle, S.; Mews, A.; Morokuma, K. *J. Phys. Chem. A* 2002, 106, 11973-11980.
87. Fleming, I. *Frontier Orbitals and Organic Chemical Reactions*; John Wiley & Sons, Ltd.: New York, 1976.
88. Kim, K. H.; Han, Y.-K.; Jung, J. *Theor. Chem. Acc.* 2005, 113, 233-237.
89. Matsuo, Y.; Tahara, K.; Nakamura, E. *Org. Lett.* 2003, 5, 3181-3184.
90. Cornell, W. D.; Cieplak, P.; Bayly, C. I.; Gould, I. R.; Kenneth M. Merz, J.; Ferguson, D. M.; Spellmeyer, D. C.; Fox, T.; Caldwell, J. W.; Kollman, P. A. *J. Am. Chem. Soc.* 1995, 117, 5179-5197.